# Dispersion characteristics of nanometer-scaled silicon rib waveguides

**Lianxi Jia (贾连希)*, Minming Geng (耿敏明), Lei Zhang (张 磊), Lin Yang (杨 林), Ping Chen (陈 平), and Yuliang Liu (刘育梁)**

*Optoelectronic System Laboratory, Institute of Semiconductors, Chinese Academy of Sciences, Beijing 100083, China*

**E-mail: jialx@semi.ac.cn*

Received October 28, 2009

We investigate the dispersion properties of nanometer-scaled silicon waveguides with channel and rib cross section around the optical fiber communication wavelength and systematically study their relationship with the key structural parameters of the waveguide. The simulation results show that the introduction of an extra degree of freedom in the rib depth enables the rib waveguide more flexible in engineering the group velocity dispersion (GVD) compared with the channel waveguide. Besides, we get the structural parameters of the waveguides that can realize zero-GVD at 1550 nm.

*OCIS codes:* 130.4310, 230.7370, 260.2030.

*doi: 10.3788/COL20100805.0485.*

Silicon photonics has attracted much attention in the past several decades due to the high-refractive-index contrast which results in a tight confinement to light and the compatibility to the complementary-metal-oxide-semiconductor (CMOS) fabrication process. The properties of the silicon waveguide, including the mode, polarization, and loss characteristics, have been widely studied[1−7]. and a lot of different devices have been fabricated based on the silicon waveguide[8−10]. With the development of the CMOS fabrication technology, the cross section of the silicon waveguide can be down to nanometer-scale but the waveguide still retains relatively low loss. So the field intensity inside the nanometer-scaled waveguide can be very high so that it could be a good candidate for the nonlinear optical devices. Meanwhile, the rapid advance in understanding the nonlinear effect in the silicon waveguide[11−20] makes the dispersion property of the waveguide become an important factor to be considered. Different nonlinear effects require different dispersion properties. For example, the soliton propagation and the supercontinuum generation require the waveguide to have proper anomalous dispersion[11−13]. The frequency expansion of the pulse wave caused by self-phase modulation (SPM) requires the waveguide to have high normal dispersion[11,12]. Effective four-wave-mixing (FWM) must satisfy phase-matching condition, which requires the waveguide to have near-zero anomalous dispersion[15−17]. In order to realize the nonlinear effects aforementioned, we need to engineer the dispersion properties of the waveguide to meet different requirements. A lot of effort has been made to study the dispersion characteristics of the channel waveguide[11−13,16−24]. However, due to the two-photon-absorption effect, there is obvious free carrier accumulation in the waveguide with high light power, which produces large absorption to the light wave and changes the refractive index of the material[25]. Though the free carrier dispersion effect is widely used in the silicon waveguide to realize the modulator[8], the impact of the free carrier dispersion effect on the high-order dispersion of the waveguide is negligible compared with the effect of the waveguide confinement[25]. So the absorption effect of the free carrier is more detrimental to the nonlinear effect in the silicon waveguide. An effective method to suppress the carrier accumulation is to form a positive-intrinsic-negative (PIN) structure in the waveguide and apply an inversely biased field to extract the carrier out of the waveguide[26,27]. So a rib structure is necessary to constrain the free carrier absorption, but the dispersion characteristics of the rib waveguide have not been thoroughly explored yet except for brief mention in Refs. [11,17]. In this letter, we systematically analyze the dispersion properties of the rib waveguide through the comparison with the channel waveguide.

We numerically investigate the group velocity dispersion (GVD) of the waveguides with channel and rib cross section around the wavelength for optical fiber communication and systematically study its relationship with the key structural parameters of the waveguide. Particular attention is paid to the GVD of the waveguide at the wavelength of 1550 nm owing to the possible application in optical fiber communication.

We investigate the silicon waveguide with rib and channel cross section as shown in Fig. 1. The inner height of the waveguide is $H$, the width of the waveguide is $W$, the slab height of the waveguide is $h$, and the ratio of the inner height to the slab height is defined as $r = h/H$. When $r = 0$, it corresponds to a channel waveguide, otherwise, it corresponds to a rib waveguide. Because the dispersion properties of the large-dimensional rib waveguides have been studied by Yin *et al.*[11] using the effective-index method which is only effective for the waveguide with large dimensions, our work is focused on the rib waveguide with the dimensions down to 1 $\mu$m or less. In this letter, the up- and bottom-cladding layers are fused silica and are considered to be infinitely thick in the simulation to ignore the possible leakage of the optical field[21].

The total dispersion of the waveguide originates from three parts: material dispersion, waveguide dispersion, and birefringence dispersion. In the nanometer-scaled

1671-7694/2010/050485-05 © 2010 Chinese Optics Letters

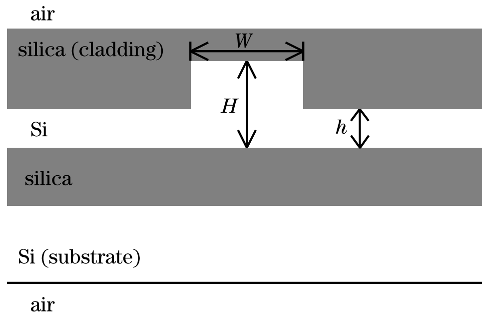


Fig. 1. Schematic diagram for the cross section of the nanometer-scaled silicon waveguide.

silicon waveguide, the material dispersion is intrinsic and determinate. The waveguide dispersion corresponds to the degree of light confinement of the waveguide and can be tailored by changing the waveguide dimensions. This is the main reason why the waveguides with different structural parameters have different dispersion properties. The birefringence dispersion is caused by the different degrees of light confinement to the different polarizations. It is so large in the nanometer-scaled waveguide that it is far beyond other two factors[19]. However, only single polarization is maintained in most of applications[11−14,16−25], so we focus our discussion on the low-loss quasi-TE single polarization in which the birefringence dispersion disappears.

In our simulation, a three-dimensional full-vector beam propagation algorithm is employed to obtain the modal effective index $n_{\text{eff}}$ $(\omega)$ numerically for the fundamental quasi-TE mode. Then, the modal propagation constant $\beta$ $(\omega)$ at the frequency $\omega$ can be obtained through the definition $\beta$ $(\omega)= n_{\text{eff}}/c$, where $\omega$ is the angular frequency of the light and $c$ is the light speed in vacuum. In order to study the dispersion properties, we use the GVD coefficient $\beta_2$ $(\omega)$ to represent the second-order dispersion effect of the waveguides, which is defined as the second-order derivative of the modal propagation constant with respect to the angular frequency[16]:

$$\beta_2(\omega) = \frac{\mathrm{d}^2\beta(\omega)}{\mathrm{d}\omega^2}. \tag{1}$$

When $\beta_2(\omega) > 0$, it is called normal dispersion, otherwise, it is anomalous dispersion. The validity of this procedure is verified in Refs. [13,17,18,20].

In this work, silicon and fused silica are the dielectric materials. In order to obtain accurate results of the high-order dispersion effects, it is necessary to take account of the material dispersion. We assume the refractive index to be isotropic and model the material dispersion using the Sellmeier model. For fused silica, the Sellmeier equation is

$$n_{\mathrm{SiO_2}}^2 = 1 + \sum_{j=1}^{M} \frac{B_j \lambda^2}{\lambda^2 - \lambda_j^2}, \tag{2}$$

where the coefficients $B_1$=0.6961663, $B_2 = 0.4079426$,$B_3 = 0.8974794$ and the reference wavelengths $\lambda_1 = 0.0684043$ $\mu$m, $\lambda_2 = 0.2262414$ $\mu$m, $\lambda_3 = 9.8961663$ $\mu$m[15]. For silicon, the Sellmeier equation is

$$n_{\mathrm{Si}}^2 = \varepsilon_1 + \frac{A}{\lambda^2} + \frac{B\lambda_1^2}{\lambda^2 - \lambda_1^2}, \tag{3}$$

where the coefficients $\varepsilon_1$=11.6858,$A$=0.93981,$B$=8.10462 $\times 10^{-3}$, $\lambda_1$=1.1071 $\mu$m[28]. For later comparison, the material dispersion is calculated using Eq. (1) with the modal effective index replaced with the material refractive index.

Based on the above method, we calculated the propagation constant $\beta(\omega)$ of the $\mathrm{TE_0}$ mode. Then, the resulting curve was differentiated numerically using a spline-fit procedure to calculate the GVD coefficient $\beta_2(\omega)$.

We studied the wavelength-dependence of the GVD coefficient around 1550 nm. In Fig. 2, $\beta_2(\omega)$ for different waveguide dimensions are shown at the wavelength range from 1300 to 1800 nm. For comparison, the material dispersions for silicon and fused silica are also shown. It can be seen that the total GVD is changed from normal dispersion to anomalous dispersion within this spectral band, which meets the requirements of different nonlinear effects as above-mentioned. The dispersion of fused silica can be ignored compared with that of silicon and the waveguide dispersion, as shown in Fig. 2. In the short wavelength, the contribution of the waveguide dispersion for most cases shows the opposite dispersion properties compared with the silicon material dispersion, and the total dispersion curves are beneath that of silicon. Under tight confinement condition, the waveguide dispersion is anomalous and the total dispersion curve is beneath that of silicon. As the increase of wavelength, the light confinement of the waveguide gets weak and the total dispersion approaches the dispersion of silicon. We can see that there are some cross points between the total dispersion curves and the material dispersion curve of silicon, which means that the contribution of the waveguide dispersion is zero at these points. Further increase of the wavelength generates normal waveguide dispersion and

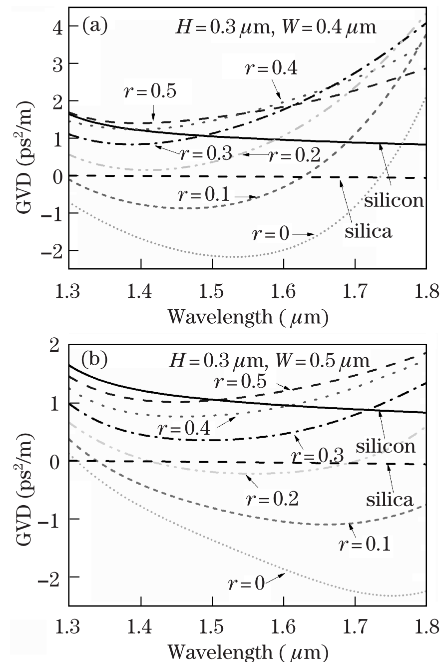


Fig. 2. Plots of the calculated GVD coefficient of the nanometer-scaled silicon waveguides with different etching depths as a function of the wavelength. The solid and dashed lines are the material dispersions of silicon and fused silica, respectively.

the total dispersion is enhanced to show larger normal dispersion than silicon material. For some waveguide dimensions, such as $H$=0.3 $\mu$m, $W$=0.4 $\mu$m, and $r$=0.5, the dispersion curve is upon the material dispersion of silicon in the whole spectral band, which means that this waveguide has a weak confinement to the light and the GVD coefficient from the waveguide dispersion is positive in this spectral band.

Figure 2 also shows the dependence of the dispersion properties of the waveguides on their structural parameters. The coefficient $r$ is in the range from 0 to 0.5, corresponding to different etching depths. As the increase of $r$, which means the decrease of the etching depth, the degree of the confinement to light weakens. So the anomalous dispersion gets small as the increase of $r$ and the total dispersion possibly shows normal dispersion. The decrease of the waveguide dispersion can also be seen from the change of the zero-dispersion wavelength (ZDWL). The material dispersion is normal, so the appearance of the ZDWL is due to the compensation of the waveguide dispersion. It is clearly shown in Fig. 2 that the ZDWL increases and gradually disappears as the increase of $r$, which means that the waveguide dispersion decreases and eventually cannot compensate for the material dispersion.

In Fig. 2, there are also some crossing points among different curves, which means that the waveguides with different structural parameters possibly have the same GVD coefficient at a certain wavelength. Besides, the decrease of $W$ from 0.5 to 0.4 $\mu$m also results in the increase of the waveguide dispersion for some spectral range but not for all, because the light confinement of the waveguide is not monotonously dependent on the dimensions of the waveguide. The impact of the waveguide dimensions on the dispersion properties of the waveguide is complicated and will be discussed detailedly next.

Based on the above analysis, we further study the dependence of the dispersion properties of the nanometer-scaled silicon waveguide on the structural parameters. We emphasize the dispersion properties at 1550 nm, which is important in optical fiber communication, but there are similar properties at other wavelengths.

The effect of the width on the GVD is analyzed, where the height of the waveguide is kept to be 0.3 $\mu$m, while the width of the waveguide, which can be changed conveniently and exactly in the fabrication process, is altered. The impact of the etching depth on the GVD is also investigated by repeating the above process with different values of $r$. As shown in Fig. 3(a), the GVD coefficient of the channel waveguide ($r$=0) is changed in a large range from −3 to 8 ps$^2$/m. The GVD coefficient is positive for W < 0.34 $\mu$m, which means that it embodies normal dispersion. As the increase of $W$, the GVD coefficient becomes negative gradually and the magnitude of the GVD coefficient can reach negative maximum at $W$=0.4 $\mu$m. With further increase of $W$, the GVD coefficient becomes positive again and approaches the GVD coefficient of silicon gradually. So there are two values of $W$=0.34 $\mu$m and $W$=0.8 $\mu$m, at which the GVD coefficients are zero. We can also see that the slope of the curve at $W$=0.8 $\mu$m is smaller, which indicates that the zero-GVD point is less susceptible to the variation of $W$ and corresponds to larger fabrication tolerance. These results are in good agreement with that in Ref.[20], in which authors deduced the dispersion properties of the channel waveguides approximately using the effective index method in a large spectral band and predicted the dependence of the GVD coefficient on the waveguide dimensions according to the theory of scale invariance of the Maxwell equations. We directly verify their conclusion and promote it to the nanometer-scaled waveguide.

Furthermore, we also find that the rib waveguide have the similar dispersion properties. However, as the increase of $r$, the maximum of the magnitude of the negative GVD coefficient decreases. In some situation, anomalous dispersion even disappears. So the etching depth must be deep enough for realizing the phase-matching demand of the FWM in rib waveguide. This result is also consistent with those in Refs. [23,24], in which the authors suggested a method to reduce the maximum of the magnitude of the negative GVD coefficient and modulate the fourth-order dispersion coefficient $\beta_4(\omega)$ through changing the refractive index of the cladding layers. But this method increases the fabrication difficulty and cannot optionally change the refractive index, which is constrained by the available cladding materials. According to the effective index method, changing the etching depth of the slab can achieve the same effect as changing the refractive index of the cladding, which is confirmed by our results, and is more convenient to be carried out in the CMOS fabrication process. Therefore, the wavelength converter based on the rib waveguide can achieve better performance than that based on the channel waveguide, since changing the etching depth of the slab of the rib waveguides cannot only control the GVD but also modulate the fourth-order dispersion simultaneously to meet the phase-matching demand in a larger bandwidth[16,23]. Besides, the rib waveguide can also form a PIN structure to suppress the free carrier absorption[26,27], which is the main constrain of

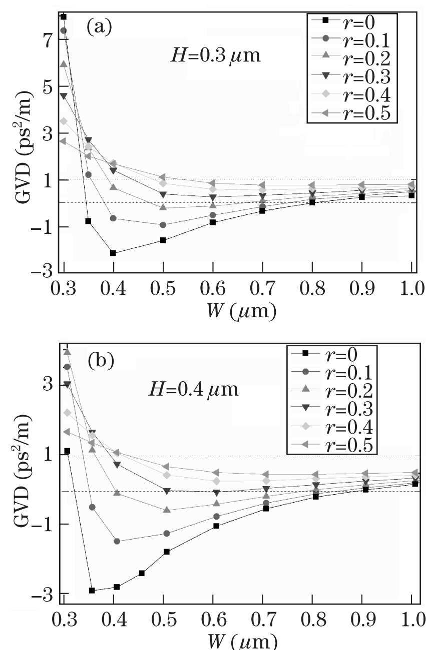


Fig. 3. Dependence of the GVD coefficient on the width of the nanometer-scaled silicon waveguides with different etching depths at 1550 nm.

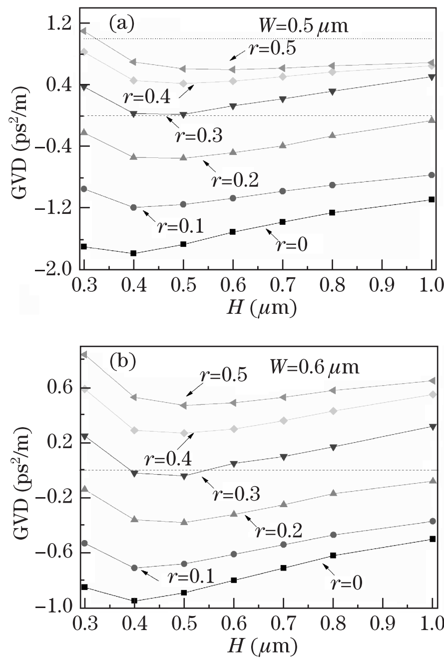


Fig. 4. Dependence of the GVD coefficient on the height of the nanometer-scaled silicon waveguides with different etching depths at 1550 nm.

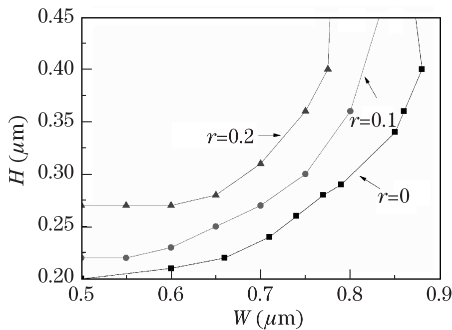


Fig. 5. Contour map of the zero-GVD for the nanometer-scaled silicon waveguides at 1550 nm.

improving the conversion efficiency as the increase of the pump power[29].

It is also shown in Fig. 3 that the maximum of the normal GVD coefficient is also dependent on $r$: the deeper the etching depth, the greater the normal GVD coefficient. This information is important for designing all-optical regenerator based on the frequency expansion, which is induced by the SPM and the relatively large normal dispersion[14]. From our simulation, we can make out that small and deeply etched structures are more appropriate for realizing such application at the cost of more precise fabrication process because of the steeper slope of the curves. For confirming the validity of the results, the simulations were repeated by keeping the height to be 0.4 $\mu$m. The results are shown in Fig. 3(b), which displays the similar properties as in Fig. 3(a) but the GVD coefficient of the waveguides covers a relatively small range.

For the completeness of the research, the effect of the height on the GVD is also studied in the similar method. $W$ is set to be 0.5 and 0.6 $\mu$m. The results are shown in Fig. 4. As $H$ increases, the GVD coefficient has the similar tendency to the case of changing $W$ but in a less significant range, which indicates that the impact of $H$ on GVD is less obvious than that of $W$, because the simulation is focused on the TE polarization. So adjusting the width is a more effective method to control the GVD of the waveguide in the wider range.

Finally, the zero-GVD contours at 1550 nm are created. From Figs. 3 and 4, we can see that not all the waveguides exhibit zero-GVD but those with deep enough etching depth do. Figure 5 shows the zero-GVD contours for $r$ limited to be 0, 0.1, and 0.2, where $H$ ranges from 0.2 to 0.45 $\mu$m and $W$ ranges from 0.4 to 0.9 $\mu$m. For some heights, two widths exist for zero-GVD as shown in Fig. 3. Here, we present the wider value for the reason mentioned before. The zero-GVD contours of the channel waveguide are in agreement with the results of the recent work by Dadap *et al.*[13] If we want to design a waveguide with zero-GVD at 1550 nm, we had better chosen that with small height, which can make the width endure relatively high fabrication tolerance.

We have presented the numerical analysis of the GVD properties of the nanometer-scaled silicon waveguide with channel and rib cross section. Through extensive simulation, the impact of the key structural parameters of the waveguide on GVD is studied. The results show that the rib waveguide, which has an extra degree of freedom in the etching depth compared with the channel waveguide, has more advantages in engineering GVD.

Based on the simulation, we suggest a convenient method to optimize the performance of the wavelength conversion based on FWM in the rib waveguide and some ways for designing the proper waveguides in order to realize some other nonlinear effects effectively. Besides, the GVD at 1550 nm can be varied in the range from large anomalous value to large normal value, so that many nonlinear applications can be realized in the properly designed silicon waveguide. We also get the structural contours of the waveguides that can realize zero-dispersion at 1550 nm.

This work was supported by the National Natural Science Foundation of China (Nos. 60877015, 60977037, and 60907001) and the National "863" Program of China (No. 2009AA03Z416).

## References


1. R. A. Soref, J. Schmidtchen, and K. Petermann, IEEE J. Quantum Electron. **27,** 1971 (1991).
2. A. G. Rickman, G. T. Reed, and F. Namavar, J. Lightwave Technol. **12,** 1771 (1994).
3. K. K. Lee, D. R. Lim, H. Luan, A. Agarwal, J. Foresi, and L. C. Kimerling, Appl. Phys. Lett. **77,** 1617 (2000).
4. O. Powell, J. Lightwave Technol. **20,** 1851 (2002).
5. L. Vivien, S. Laval, B. Dumont, S. Lardenois, A. Koster, and E. Cassan, Opt. Commum. **210,** 43 (2002).
6. F. Grillot, L. Vivien, S. Laval, D. Pascal, and E. Cassan, IEEE Photon. Technol. Lett. **16,** 1661 (2004).
7. Y. A. Vlasov and S. J. McNab, Opt. Express **12,** 1622 (2004).
8. A. Liu, R. Jones, L. Liao, D. Samara-Rubio, D. Rubin, O. Cohen, R. Nicolaescu, and M. Paniccia, Nature **427,** 615 (2004).
9. K. Sasaki, F. Ohno, A. Motegi, and T. Baba, Electron. Lett. **41,** 801 (2005).

10. M. Geng, L. Jia, L. Zhang, L. Yang, P. Chen, T. Wang, and Y. Liu, Opt. Express **17,** 5502 (2009).
11. L. Yin, Q. Lin, and G. P. Agrawal, Opt. Lett. **31,** 1295 (2006).
12. L. Yin, Q. Lin, and G. P. Agrawal, Opt. Lett. **32,** 391 (2007).
13. J. I. Dadap, N. C. Panoiu, X. Chen, I. Hsieh, X. Liu, C. Chou, E. Dulkeith, S. J. McNab, F. Xia, W. M. J. Green, L. Sekaric, Y. A. Vlasov, and R. M. Osgood, Jr., Opt. Express **16,** 1280 (2008).
14. R. Salem, M. A. Foster, A. C. Turner, D. F. Geraghty, M. Lipson, and A. L. Gaeta, Opt. Express **15,** 7802 (2007).
15. G. P. Agrawal, *Nonlinear Fiber Optics* (Academic Press, San Diego, 1989).
16. M. A. Foster, A. C. Turner, J. E. Sharping, B. S. Schmidt, M. Lipson, and A. L. Gaeta, Nature **441,** 960 (2006).
17. Q. Lin, J. Zhang, P. M. Fauchet, and G. P. Agrawal, Opt. Express **14,** 4786 (2006).
18. X. Chen, N. C. Panoiu, and R. M. Osgood, Jr., IEEE J. Quantum Electron. **42,** 160 (2006).
19. V. Raghunathan, R. Claps, D. Dimitropoulos, and B. Jalali, J. Lightwave Technol. **23,** 2094 (2005).
20. I. Hsieh, X. Chen, J. I. Dadap, N. C. Panoiu, and R. M. Osgood, Jr., Opt. Express **14,** 12380 (2006).
21. E. Dulkeith, F. Xia, L. Schares, W. M. J. Green, and Y. A. Vlasov, Opt. Express **14,** 3853 (2006).
22. A. C. Turner, C. Manolatou, B. S. Schmidt, M. Lipson, M. A. Foster, J. E. Sharping, and A. L. Gaeta, Opt. Express **14,** 4357 (2006).
23. M. R. E. Lamont, B. T. Kuhlmey, and C. M. de Sterke, Opt. Express **16,** 7551 (2008).
24. X. Liu, W. M. J. Green, X. Chen, I. Hsieh, J. I. Dadap, Y. A. Vlasov, and R. M. Osgood, Jr., Opt. Lett. **33,** 2889 (2008).
25. Q. Lin, O. J. Painter, and G. P. Agrawal, Opt. Express **15,** 16604 (2007).
26. Y. Kuo, H. Rong, V. Sih, S. Xu, and M. Paniccia, Opt. Express **14,** 11721 (2006).
27. D. Dimitropoulos, S. Fathpour, and B. Jalali, Appl. Phys. Lett. **87,** 261108 (2005).
28. H. H. Li, J. Phys. Chem. Ref. Data **9,** 561 (1980).
29. K. Yamada, H. Fukuda, T. Tsuchizawa, T. Watanabe, T. Shoji, and S. Itabashi, IEEE Photon. Technol. Lett. **18,** 1046 (2006).